3 Results

3.1 Model drift and equilibration

Before evaluating the climatological performance of the simulations, we assess the degree of equilibration of the coupled system under constant forcing. While AWI-CM3-LR exhibits a clearly positive top-of-atmosphere (TOA) radiative imbalance since the beginning of the simulation, AWI-CM3-MR starts with near-zero values; both simulations, however, display a declining trend during the spin-up phase (Figure 1a,b). After spin-up, the imbalance stabilizes at approximately +0.2 W m^{-2} in the low-resolution configuration, reasonably on the lower of CMIP6 models average and reference estimates for the present-day climate (Johnson et al., 2016; Wild, 2020),, and at a nearly symmetric negative value ($\sim$-0.24 W m^{-2}) in the medium-resolution case. The surface energy imbalance is smaller in the LR simulation and more pronounced in the MR configuration, but in both cases it closely follows the evolution of the TOA flux. The relatively stable TOA–surface difference indicates that the atmospheric column remains internally consistent, while suggesting that, particularly in the MR simulation, the residual energy imbalance is primarily associated with ongoing ocean adjustment.

In both configurations, the global-mean ocean temperature bias exhibits a relatively stable vertical structure (Figure 1c,d). However, differences emerge in both the temporal evolution and the magnitude of these biases. In the LR simulation, a weak cold bias around 100 m is present during the initial adjustment phase and diminishes over time as warm biases at intermediate depths become more pronounced. This is accompanied by a persistent subsurface warming throughout the control period, indicating a sustained drift in the ocean interior despite the near-stationary behavior of the global energy budget, broadly consistent with Streffing et al. (2022). In contrast, the HR simulation shows a more stable depth-dependent pattern and less pronounced ocean temperature drift, with weaker subsurface warming and a clear upper-ocean cooling, consistent with a net upward energy flux at both the surface and the TOA.

While the low-resolution simulation can be considered reasonably equilibrated by 1950, the medium-resolution configuration still exhibits signs of residual imbalance at the time the transient simulations are branched off. This is reflected in the larger variability of the radiative balance and is consistent with the presence of an eddy-permitting ocean. Explicitly resolving mesoscale processes substantially increases the timescale required for the deep ocean to adjust (Danabasoglu et al., 1996). As a result, the approach to equilibrium is slower, and residual imbalances can persist over longer periods compared to lower-resolution configurations relying on parameterized processes (Danek et al., 2019).

Contrasts between low- and high-resolution configurations have been reported in HighResMIP and other multi-model studies, where increasing resolution leads to a reorganization, or even a reversal in sign, rather than a systematic reduction of model errors (Bock et al., 2020; Moreno-Chamarro et al., 2022).. However, most relevant for the present comparison is that both simulations exhibit an overall limited and well-constrained drift from 1950 onwards. This is evident in the weak trends of global-mean sea surface temperature and near-surface air temperature, as well as in the relatively stable sea ice extent across seasons and regions (Figure 2).

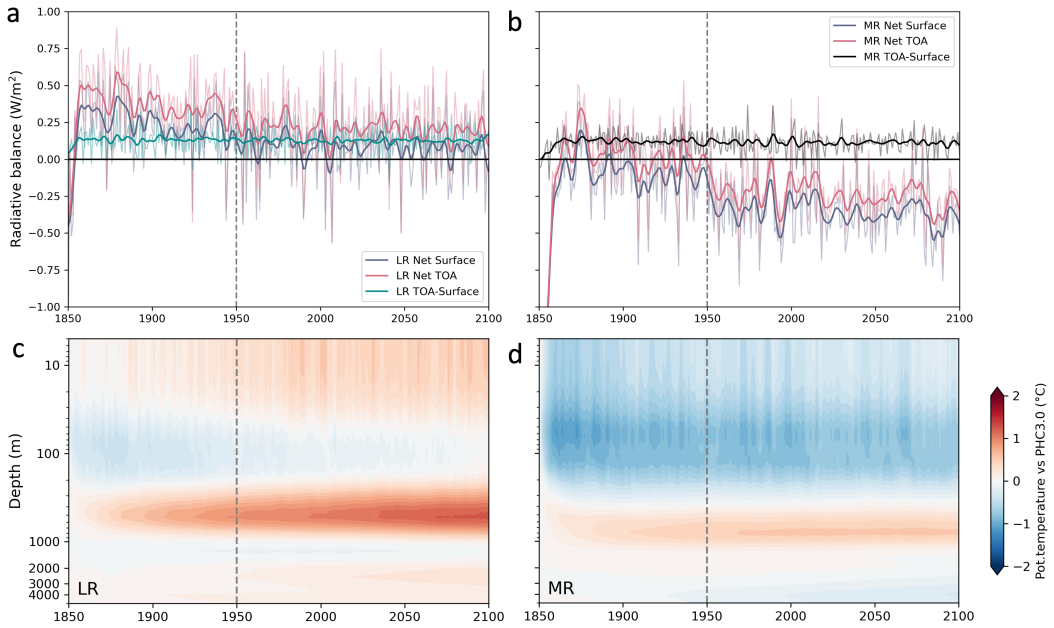

Figure 1. (a,b) Net radiative imbalance at the top of the atmosphere (TOA) and at the surface, together with their difference, representing the atmospheric column energy balance, during the spin-up and control simulations. Positive (negative) values indicate downward (upward) fluxes. (c,d) Hovmöller diagrams of the evolution of global-mean ocean potential temperature bias during the spin-up and control simulations, relative to the PHC3.0 climatology. The vertical dashed line marks the branch-off point of the transient simulations. Results are shown for the low-resolution (LR, left panels) and medium-resolution (MR, right panels) configurations.

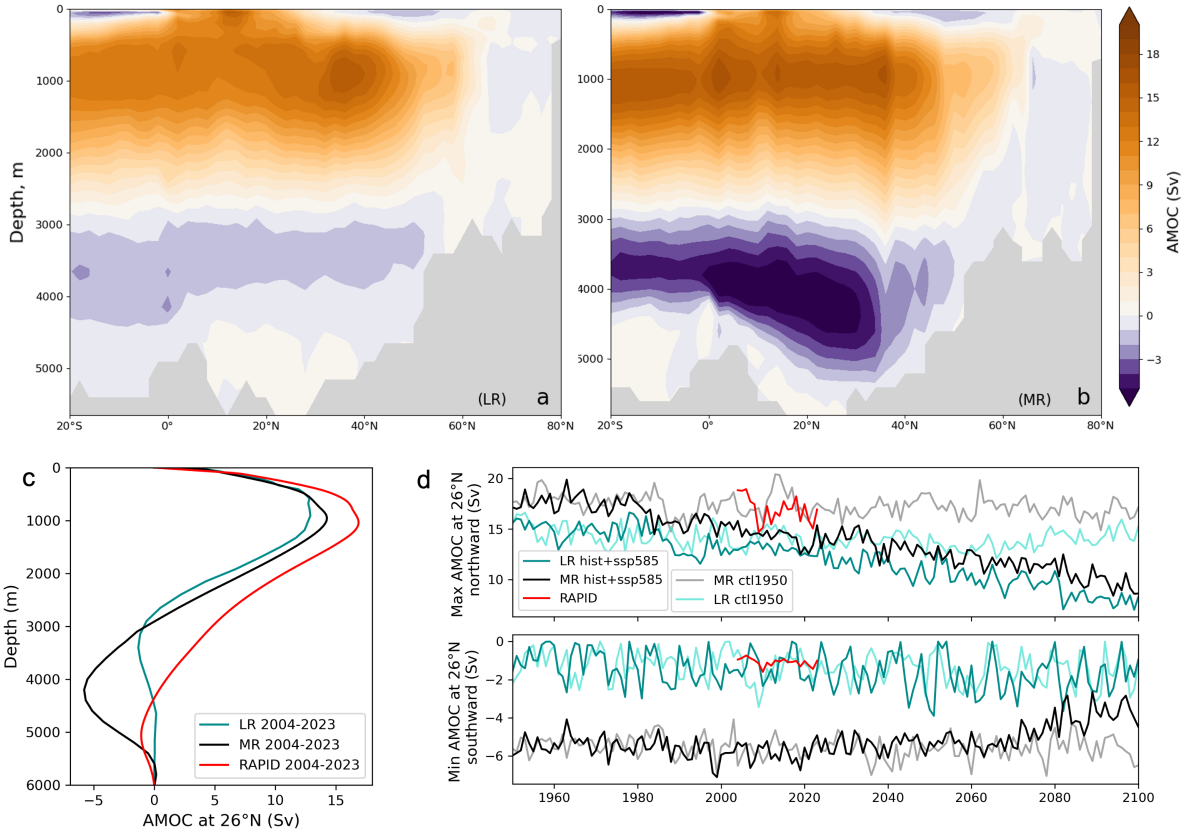

Figure 8. Atlantic Meridional Overturning Circulation (AMOC) overturning streamfunction averaged over the period 1979–2014 for (a) the low-resolution simulation (LR) and (b) the medium-resolution simulation (MR). (c) Comparison of AMOC overturning streamfunctions from AWI-CM3 simulations and RAPID-MOC array (**?**) observations at 26.5°N, averaged over the period 2004–2023. (d) Time evolution of AMOC maximum (northward transport) and minimum (southward transport) at 26.5°N from AWI-CM3 simulations and RAPID observations. (Sv denotes Sverdrups; 1 Sv = 106 m^3 s^{-1})